Spatial Information Encoded Mutual Information for Nonrigid Registration

Xiahai Zhuang, David J. Hawkes, Sebastien Ourselin

Centre for Medical Image Computing, Department of Medical Physics and Bioengineering, University College London
x.zhuang@ucl.ac.uk; http://www.cs.ucl.ac.uk/staff/x.zhuang/

Abstract. We propose a new nonrigid registration method based on a unified framework of encoding spatial information in entropy measures. The encoding of spatial information improves nonrigid registration against the problems caused by intensity distortion where the registration using traditional mutual information (MI) is challenged. Using this encoding framework, we derive the new registration method, spatial information encoded mutual information (SIEMI). SIEMI registration has a similar computation complexity as the registration using traditional MI measures, but works significantly better in the nonrigid cases. We validated the registration method using brain MRI and dynamic contrast enhanced MRI of the liver. The results showed that the proposed method performed significantly better than the normalized mutual information registration.

1 Introduction

Mutual information (MI) [1,2,3] is one of the most widely studied techniques for biomedical image registration in the last fifteen years. The registration using MI measures, including the normalized forms such as the normalized mutual information (NMI) [4], has shown good robustness and wide applicability [5,6]. However, several recent works [7,8,9,10] showed that the traditional MI measures may not be appropriate in many situations for nonrigid registration.

The first common situation happens in registering *in vivo* medical images, which have *intensity non-uniformity* (INU), also referred to as intensity distortion or intensity bias. This INU results in the same tissue in different positions having different intensity values, and thus some regions of the tissue having different *intensity classes*. Since patterns of INU fields vary in different images, the inconsistency of intensity classes of one tissue in two images will lead to large errors in nonrigid registration. Fig. 1 shows an example of registering two initially aligned brain MR images, where one contains INU while the other does not. The nonrigid registration using NMI measure [4] generates a large erroneous resultant deformation field. Fig. 1 (d) shows a more promising result using the proposed method which will be described later. This method demonstrates a much better robustness against the INU field.

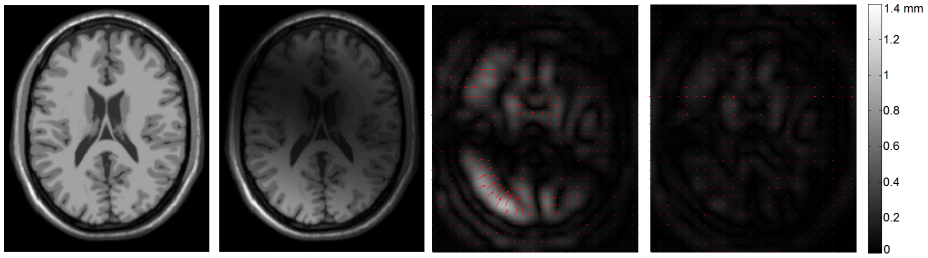

Fig. 1. (a) T1-weighted brain image without intensity non-uniformity (INU) and (b) the INU field computed from the subtraction of (a) and the image with INU. (c) is the resultant deformation field of registering (a) to the image with INU using NMI measure and (d) is the result using the proposed registration method. The color bar indicates the displacement magnitude in (c) and (d). Brain data downloaded from BrainWeb (www.bic.mni.mcgill.ca/brainweb/)

Other situations include the nonrigid registration of dynamic contrast enhanced MRI [11], perfusion MRI [12], and multi-modality images such as the CT-MR registration application [9]. It is still challenging to employ traditional MI measures for the nonrigid registration of these tasks.

To tackle the problems, Studholme *et al.* and Loeckx *et al.* proposed to consider the spatial coordinate as an extra channel of information and combine this information with the MI measure such as the regional mutual information (RMI) [7] and the conditional mutual information (cMI) [8,9]. The cMI measure was shown to be equivalent to the derived measure of RMI, referred to as RMI′ in [7], by using a different Parzen window estimation function for the spatial variable [9,10]. Loeckx *et al.* further showed that the cMI registration performed better than the registration using the original RMI similarity form [9].

In this work, we extend the generalized weighting scheme for spatial information encoding in the previous work [10] to propose a new registration method. The weighting scheme is to vary the contribution of pixels to a set of joint histogram tables which are associated with a spatial variable. The registration measure, spatial information encoded mutual information (SIEMI), is a vector consisting of a set of entropy measures computed from these joint histogram tables.

The rest of the paper is organized as follows: Section 2 presents the SIEMI method; Section 3 provides the validation experiments, where discussion is also included; finally, our conclusions are given in Section 4.

2 Method

2.1 Definition of terms and notations

Intensity distribution: Intensity distribution describes the appearance and contrast of organs or tissues presented in a medical image.

Intensity class: We assume that the imaged intensity values in our registration images, such as MRI data, are related to the tissue types. Therefore, in an image scanned from n_{tis} types of tissues, n_{tis} intensity values should be presented. However, the intensity of one tissue normally has an intensity range in *in vivo* scans due to the non-uniformity of tissue property and noise. Also, a number of different tissues, referred to as a class of tissues, may have their intensity ranges overlapped. Hence, the intensity distribution is presented as n_C classes of intensity ranges, referred to as intensity classes.

Global intensity class linkage: The intensity class correspondence, reflecting the true joint intensity distribution of the two images, is normally unknown before registration due to the misalignment in local regions. By assuming the two images initially close to a true match and considering the local misalignment as noise, we can estimate this correspondence using the approximated joint intensity distribution from the global intensity information of the two images [13]. This global information, providing important guidance for correcting misaligned local regions, is referred to as *global intensity class linkage*.

Spatial variable s and local region Ω_s: Spatial variable s is an index of a set of spatial positions, $s = 1 \ldots n_s$. The positions are defined according to the nonrigid transformation parameters. For example, in fluid registration each pixel (or voxel) can be defined as a value of spatial variable, while in free-form deformation (FFD) registration each control point can be defined as a value of s. It is commonly to define a local region Ω_s for s such as the user-defined cubic regions [7] or the local support volume of the FFD control point [8].

2.2 The framework of spatial information encoding

Spatial information encoding is achieved by varying the contribution of pixels to a set of joint histogram tables $\{\mathcal{H}_s\}$, from which a set of entropy measure $\{\mathcal{S}_s\}$ are computed, as illustrated in Fig. 2. The contribution is according to the spatial coordinate of the pixel and value of s.

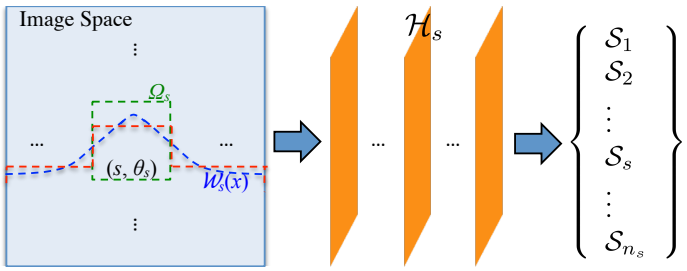

Fig. 2. The spatial variable s, associated local region Ω_s, transformation parameter θ_s, weighting function $\mathcal{W}_s(x)$, joint histogram table $\mathcal{H}_s$, and entropy measure $\mathcal{S}_s$. The spatial information encoded similarity measure is the vector representation of $\{\mathcal{S}_s\}$.

Let I_r be the reference image, I_f^T be the transformed floating image by transformation T, θ_s be a parameter of T, and Ω_s be the user-defined local region. Both θ_s and Ω_s are associated with the spatial variable s. To compute $\mathcal{S}_s$, we can estimate the local histogram using the information solely within the local region Ω_s, referred to as *local information*. However, the size of the local region Ω_s may be very small compared to the global volume Ω, which potentially leads to two problems. One is that the estimation of local probability distribution functions (PDFs) using a small number of sample points may lose the statistical power of the computed local entropy measure $\mathcal{S}_s$ [14,15]. The other is that this estimation of local PDFs may lose the global intensity class linkage [16,17]. Both of the two problems will result in reduced registration robustness using the local entropy measures.

To deal with the limitation of solely using local information, Likar and Pernus proposed to combine the local estimation with the global estimation [15]:

$$p_s(r,f) = wp_{_L} + (1-w)p_{_G} \ , \tag{1}$$

where $p_{_L} = \frac{1}{N_{_L}} \sum_{x\in\Omega_s} \omega_r(I_r(x))\omega_f(I_f^T(x))$ is estimated from Ω_s and $p_{_G} = \frac{1}{N_{_G}} \sum_{x\in\overline{\Omega}_s} \omega_r(I_r(x))\omega_f(I_f^T(x))$ is estimated from the complementary volume $\overline{\Omega}_s$, referred to as the *global information*; ω_r and ω_f are Parzen window estimation functions and $N_{_L}$ and $N_{_G}$ are the normalization factors. The weighting is set as $w = \frac{N_{_L}}{N_{_L}+N_{_G}}$, proportional to the volume size of the local region Ω_s [15].

To assess the weights of each sample point $x \in \Omega$, Eq. (1) is rewritten:

$$p_s(r,f) = \frac{1}{N} \sum_{x\in\Omega_s} \omega(\circ)\frac{wN}{N_{_L}} + \frac{1}{N} \sum_{x\in\overline{\Omega}_s} \omega(\circ)\frac{(1-w)N}{N_{_G}} \ , \tag{2}$$

where $\omega(\circ) = \omega_r(I_r(x))\omega_f(I_f^T(x))$ and $N = N_{_L} + N_{_G}$. The weighting function is then given by:

$$\mathcal{W}_s(x) = \begin{cases} \frac{wN}{N_{_L}}, & x \in \Omega_s \\ \frac{(1-w)N}{N_{_G}}, & x \in \overline{\Omega}_s \end{cases} \ . \tag{3}$$

By using the setting in [15], the weights of all points $x \in \Omega$ are then the same, $\frac{wN}{N_{_L}} = \frac{(1-w)N}{N_{_G}} = 1$, resulting in the same value for all computed local measures, $\mathcal{S}_1 = \mathcal{S}_2 = \cdots = \mathcal{S}_{n_s}$, and no spatial information being encoded in $\{\mathcal{S}_s\}$.

Therefore, we can use $w \in [N_{_L}/N, 1]$ to generalize the weighting scheme [10]. The weighting function is illustrated as the red dash-line in Fig. 2. This scheme has the mechanism of maintaining the global intensity class linkage as well as differentiating local regions in the computation of $\{\mathcal{S}_s\}$. However, the disadvantage is that all sample points within the local region Ω_s have the same weight, $wN/N_{_L}$, regardless their different spatial coordinates.

Therefore, we propose to generalize the weighting scheme such that the value of $\mathcal{W}_s(x)$ should be monotonically decreasing with respect to the distance between x and the coordinate of s. This weighting function is illustrated as the

blue dash-line in Fig. 2. The spatial variable associated joint histogram table is then given by:

$$\mathcal{H}_s(r,f) = \sum_{x\in\Omega} \omega_r(I_r(x))\omega_f(I_f^T(x))\mathcal{W}_s(x) \ . \tag{4}$$

Accordingly, the joint PDF is computed as $p_s(r,f) = \frac{1}{N_s}\mathcal{H}_s(r,f)$, where $N_s = \sum_{r,f}\mathcal{H}_s(r,f)$ is the normalization factor. Given $s = x$, the estimated PDF turns out to be similar to the local PDF in [13].

The derivative of $\mathcal{H}_s(r,f)$ with respect to a transformation parameter θ_t is given by:

$$\frac{\partial\mathcal{H}_s(r,f)}{\partial\theta_t} = \sum_{x\in\Omega_t} \frac{\partial\omega_f(I_f^T(x))}{\partial\theta_t}\omega_r(I_r(x))\mathcal{W}_s(x) \ , \tag{5}$$

where Ω_t is the local support volume of θ_t. The computation of $\partial\omega_f(I_f^T(x))/\partial\theta_t$ is the same as that in the traditional MI registration [1,2,3]. The computation complexity of Eq. (5) is $O(|\Omega_t|)$. Finally, the computation for marginal histogram tables and PDFs is similar, based on which MI or the normalized measures and their derivatives are computed.

2.3 Spatial information encoded mutual information

Similarity measure: The set of entropy measures $\{\mathcal{S}_s\}$ is computed from their associated PDFs. This computation results in a vector measure composed of $\{\mathcal{S}_s\}$ between the two registration images, as Fig. 2 shows. We refer to this measure as the *spatial information encoded mutual information* (SIEMI):

$$\text{SIEMI} = \{\mathcal{S}_1, \mathcal{S}_2, \cdots, \mathcal{S}_s, \cdots, \mathcal{S}_{n_s}\}^{\mathrm{T}} \ , \tag{6}$$

To present a scalar value of SIEMI, one scheme is to compute the weighted sum of $\{\mathcal{S}_s\}$:

$$\text{SIEMI}_{\text{sum}} = \sum_s p(s)\mathcal{S}_s \ , \tag{7}$$

where $p(s) = N_s/\sum_t(N_t)$.

Alternatively, since SIEMI is a vector, the squared magnitude of the vector can be computed as a scalar similarity measure:

$$\text{SIEMI}_{\text{mag}} = \sum_s \left(\mathcal{S}_s\right)^2 \ . \tag{8}$$

The entropy measure $\mathcal{S}_s$ can be the joint entropy, MI, or the normalized forms such as NMI [4] and entropy correlation coefficient [2]. Studholme *et al.* [4] showed that NMI was robust to the changes in overlap volumes. Therefore, we use NMI for the implementation of $\mathcal{S}_s$ in this work. Noted that the results of using other MI forms may not be significantly different.

Driving forces and optimization of SIEMI: Given a nonrigid transformation parameter θ_s, the steepest ascent direction of registration using the scalar SIEMI is given by the derivative of SIEMI in Eq. (7) or Eq. (8) as follows:

$$\begin{aligned} \boldsymbol{F}_{SA}(\theta_s) &\equiv \frac{\partial \text{SIEMI}}{\partial \theta_s} \\ &= \sum_t \frac{\partial C(\mathcal{S}_t)}{\partial \theta_s}, \text{where } C(\mathcal{S}_t) \text{ is } (\mathcal{S}_t)^2 \text{ or } p(t)\mathcal{S}_t \ . \end{aligned} \tag{9}$$

The computation complexity of Eq. (9) is $O(n_s \cdot |\Omega_s|)$, where n_s is the number of the spatial variable values. However, this computation may be practically too expensive when n_s is large, compared to only $O(|\Omega_s|)$ in standard MI.

Since SIEMI is a vector of $\{\mathcal{S}_s\}$, we propose to optimize each $\mathcal{S}_s$ with respect to θ_s using a direction of local ascent, resembling a greedy strategy:

$$\boldsymbol{F}_{LA}(\theta_s) \equiv \partial \mathcal{S}_s / \partial \theta_s \ . \tag{10}$$

The computation complexity of Eq. (10) is now *significantly reduced* to $O(|\Omega_s|)$, which compares with $O(n_s|\Omega_s|)$ of Eq. (9). This *local ascent optimization* assumes that the optimization of each $\mathcal{S}_s$ would not deteriorate that of others, and thus would globally converge. The convergence of local ascent optimization, along with the comparisons with using global ascent optimization for $\text{SIEMI}_{\text{sum}}$, $\text{SIEMI}_{\text{mag}}$, and NMI, will be validated in Section 3.1.

2.4 Choices of $\mathcal{W}_s(x)$ and unifying existing works

The spatial variable s is defined according to the nonrigid transformation model used in the registration. In this work, we employ the free-form deformations (FFDs) [5]. The value of s is defined to the index of the control points of FFD grids, and Ω_s is the local support volume of the control point.

Spatial information encoding is determined by the weighting scheme $\mathcal{W}_s(x)$. By using constant value such that $\mathcal{W}_s(x) = 1$, the computed measure $\mathcal{S}_s$ is identical to traditional entropy measure such as the MI or NMI.

By using the *boxcar* function, the 0-order B-spline function β^0:

$$\mathcal{W}_s(x) = \begin{cases} 1, \text{if } x \in \Omega_s \\ 0, \text{otherwise} \end{cases} \tag{11}$$

the joint PDFs associated with s, $p_s(r, f)$, become the regional PDFs and the corresponding $\text{SIEMI}_{\text{sum}}$ is then given by:

$$\text{SIEMI}_{\text{sum}}|_{\mathcal{W}_s=\beta^0, \mathcal{S}_s=\text{MI}} = \sum_s p(s) \sum_{r,f} p_s(r, f) \log \frac{p_s(r, f)}{p_s(r)p_s(f)} \ , \tag{12}$$

which is identical to the derived RMI' measure proposed in [7].

By using the cubic B-spline function β^3 such that:

$$\mathcal{W}_s(x) = \beta^3_{\Delta_1}(x_1 - \phi_{s1})\beta^3_{\Delta_2}(x_2 - \phi_{s2})\beta^3_{\Delta_3}(x_3 - \phi_{s3}) \ , \tag{13}$$

the joint PDFs associated with s become the conditional PDFs $p(r, f|s)$, where $x = [x_1, x_2, x_3]^{\mathrm{T}}$ is the sample point's coordinate, $[\phi_{s1}, \phi_{s2}, \phi_{s3}]^{\mathrm{T}}$ is the coordinate of the s corresponded FFD control point, and $[\Delta_1, \Delta_2, \Delta_3]$ are the FFD spacing in each dimension. $\mathrm{SIEMI}_{\mathrm{sum}}$ then becomes the cMI in [8,9].

In this study, we use the Gaussian kernel function for $\mathcal{W}_s(x)$, in 3D as follows:

$$\mathcal{W}_s(x) = Ae^{-\left(\frac{(x_1-\phi_{s1})^2}{2\sigma_1^2}+\frac{(x_2-\phi_{s2})^2}{2\sigma_2^2}+\frac{(x_3-\phi_{s3})^2}{2\sigma_3^2}\right)}, \tag{14}$$

where $A = 1$ and $[\sigma_1, \sigma_2, \sigma_3]$ are the standard deviations. In practice, the locality of the Gaussian function is set to the volume within three times the standard deviation. Therefore, $\mathcal{W}_s(x)$ using Eq. (14) is similar to the cubic B-spline function in Eq. (13), given $\sigma_i = \frac{2}{3}\Delta_i$, where Δ_i is the FFD spacing in each dimension.

The amount of information used in the computation of $\mathcal{H}_s$ in Eq. (4) is related to the non-zero-value domain of $\mathcal{W}_s(x)$. More information corresponds to better registration robustness, while more locality means higher achievable registration accuracy. A strategy to combine them is to start the registration using $\mathcal{W}_s(x)$ with a large non-zero-value domain such as the global space and hierarchically decrease the domain. This *hierarchy scheme* can be related to the multiresolution FFD registration [18] such as by setting the none-zero-value domain to the local support of the corresponding control point [8]. In this study, we set $\sigma_i = l\Delta_i$ to regularize the locality of $\mathcal{W}_s(x)$ in the multiresolution FFDs [18]. In this scheme, the information used in the computation of $\mathcal{H}_s$ can be extended to $(1.5l)^d$ times of the local support volume of the control points, where d is the dimension. We use $l \in [1, 2]$ in our experiments, where the smallest FFD spacing is 10 mm and the minimal number of sample points for the construction of histogram tables can be easily met [19].

We notice that there are applications which may need much finer spacing FFD registration. For this situation, we need to define $[\sigma_1, \sigma_2, \sigma_3]$ of Eq. (14) to be large enough to guarantee enough sample points for the construction of $\mathcal{H}_s$, such as σ_i=10mm when $l\Delta_i$ <10mm.

It should be noted that the computation complexity of the optimization using Eq. (10) is not significantly increased along with the increased value of l. This is because it is determined by the size of local support volume as Eq. (5) shows.

3 Experiment

3.1 Global steepest ascent VS local ascent optimization

Data: This experiment uses 2D brain MR T1 images, downloaded from BrainWeb to demonstrate the difference of SIEMI registration using the steepest ascent optimization, Eq. (9), and the local ascent optimization, Eq. (10). The steepest ascent optimization was applied to NMI, SIEMI using sum of $\{\mathcal{S}_s\}$, referred to as $\mathrm{SIEMI}^{\mathrm{SA}}_{\mathrm{sum}}$, and SIEMI using magnitude of $\{\mathcal{S}_s\}$, referred to as $\mathrm{SIEMI}^{\mathrm{SA}}_{\mathrm{mag}}$. The SIEMI registration using the local ascent optimization is referred to as SIEMI.

Table 1. The registration accuracy, given by warping index (WI), of the four schemes. The table also presents the p-values of the t-test between the registration accuracy of SIEMI and that of the other three methods, and the ratios of computation time (RCT) of the other three methods to that of the SIEMI.

	NMI	$\text{SIEMI}^{\text{SA}}_{\text{sum}}$	$\text{SIEMI}^{\text{SA}}_{\text{mag}}$	SIEMI
WI (0.01 mm)	23 ± 0.9	11 ± 0.6	11 ± 0.5	11 ± 0.7
P-value	<0.0001	0.462	0.662	—
RCT	0.60	160	144	1

One of the registration images did not have INU while the other had a 20% field. The initial transformations, regarded as the ground truth for the registration accuracy assessment, were combinations of scalings and FFD transformations [5] with 45×54 mm mesh spacing. Six different scaling values were chosen between [0.95, 1.05] and the FFD transformations moved the central control points either 15 mm or -15 mm at each direction, together generating 24 initial transformations. The *warping index*, root mean square (RMS) residual displacement error, of the initial transformation fields ranged between [3.47, 4.63] (3.90 ± 0.49) mm.

The registration used a series of concatenated isotropic FFDs with two levels (spacings 20mm and 10mm) [18,20]. The registration firstly employed 100 iteration steps for the 20 mm FFD level, and then 40 steps for the 10 mm FFD level. The warping index was calculated every 10 iteration steps.

Results: Fig. 3 (left) illustrates the mean warping indexes by the four registration methods. They are displayed in every 10 iteration steps. The mean accuracy is also displayed in Table 1 where the evidently small standard deviation values, all less than 0.01 mm, indicate the consistent performance of each registration scheme in the test cases. It is evident from Table 1 that NMI registration needed the least computation time, but it achieved a much worse warping index than the other three registration schemes.

For the SIEMI registration schemes, the computation of each iteration step in SIEMI was more than 100 times faster than those of $\text{SIEMI}^{\text{SA}}_{\text{sum}}$ and $\text{SIEMI}^{\text{SA}}_{\text{mag}}$, as Table 1 shows. The optimization of SIEMI is shown to converge twice to three times slower than $\text{SIEMI}^{\text{SA}}_{\text{sum}}$ and $\text{SIEMI}^{\text{SA}}_{\text{mag}}$ (Fig. 3 (left)), but it is still much faster in overall. Furthermore, there was no statistically significant difference in terms of registration accuracy between the use of the local ascent optimization and that of the two global steepest ascent schemes, as the p-value of the two tailed, paired t-test between SIEMI and $\text{SIEMI}^{\text{SA}}_{\text{sum}}$ was 0.462, and that between SIEMI and $\text{SIEMI}^{\text{SA}}_{\text{mag}}$ was 0.662.

3.2 Performance to intensity non-uniformity

Data: This experiment employs 3D brain MR images to study the performance of NMI and SIEMI registration in different magnitudes of INU fields.

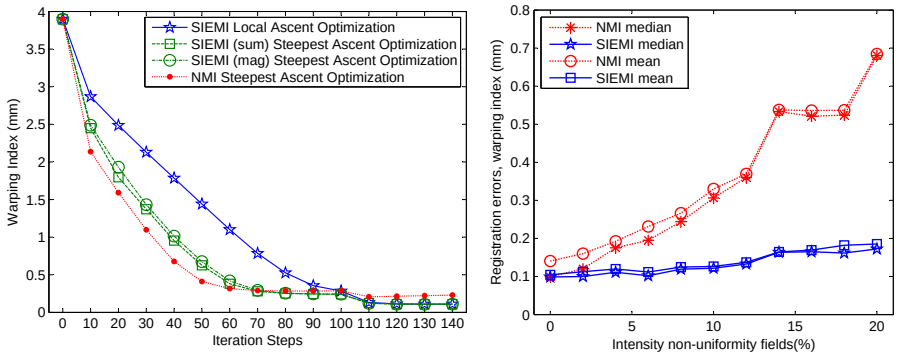

Fig. 3. The mean warping index of the 24 cases in every 10 iteration steps (left) and the mean and median values of the registration errors by SIEMI and NMI in the different intensity non-uniformity fields (right).

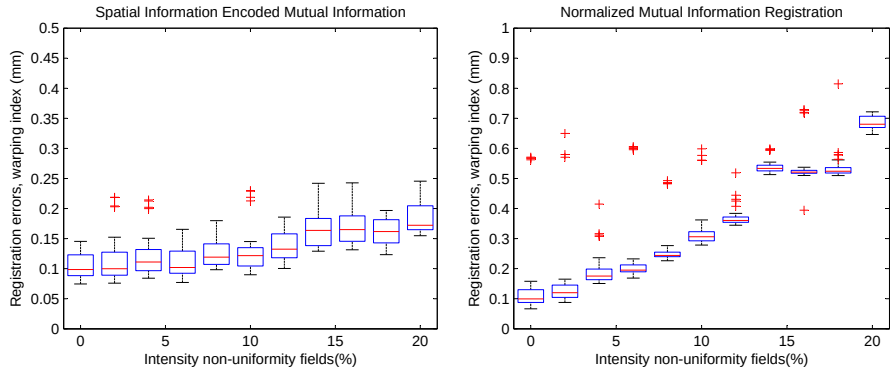

Fig. 4. The Box-and-Whisker diagrams of 48-case registration errors by SIEMI (left) and NMI registration (right) in different intensity non-uniformity fields.

The MR images were downloaded from the BrainWeb with 3% noise. Eleven levels of INU fields were generated, from 0% to 20%, using the equation $\mathcal{B} = a_1x^2 + a_2y^2 + a_3z^3 + a_4xy + a_5xz + a_6yz + a_7x + a_8y + a_9z$, where $[x, y, z]$ is the pixel coordinate, and $\{a_i\}$ are random values in $[-1, 1]$. The magnitudes of the fields were normalized to the percentage of the intensity range of the original image. Forty-eight deformation fields were generated using the same method employed in Section 3.1, where the FFD mesh used in this experiment was 3D and with $45 \times 54 \times 45$ mm spacing. These initial deformations, warping index ranging from 0.31 mm to 6.27 mm (2.67 ± 1.49 mm), were used to generate 48 registration cases for each level of the INU fields.

SIEMI and NMI registration used the same transformation model, a series of concatenated isotropic FFDs with two levels (spacings 20mm and 10mm) [18,20].

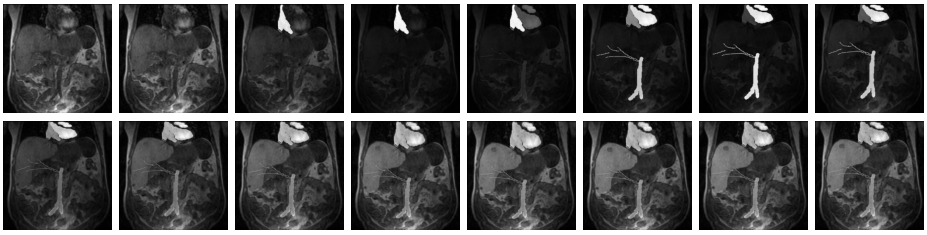

Fig. 5. One example of the simulated dynamic contrast enhanced MR data in 15 time points. The first one from the left of the upper row is the image without enhancement. The images from the second of the upper row to the second row are the dynamic enhanced data from time point one to fifteen.

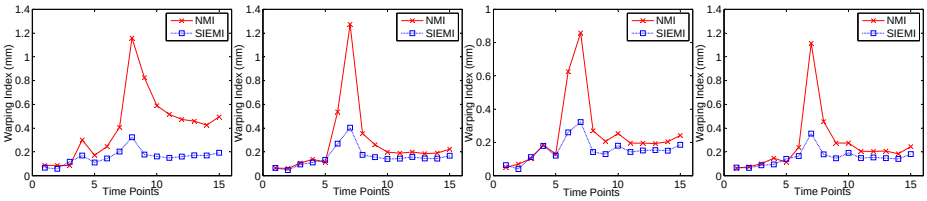

Fig. 6. The registration results, warping indexes, of the four simulated dynamic contrast enhancement MRI cases by SIEMI and NMI registration.

Results: Fig. 4 plots the Box-and-Whisker diagrams of the warping index of the 48 registration cases by NMI and SIEMI in each level of INU fields, and Fig. 3 (right) shows the mean and median numbers of them. The two registration methods achieved similar warping indexes in most of the cases in 0% INU level, but NMI had three outlier cases whose errors were larger than 0.5 mm. In the cases of images with INU, SIEMI registration performed with a fairly consistent mean warping index with respect to different levels of INU magnitudes, while NMI registration had radically increased registration errors when the INU became strong.

3.3 Application to dynamic contrast enhanced MRI

Data: This experiment employs four sets of simulated DCE MRI data where the intensity values during flush-in of the contrast agent varied as a function of time and positions. Fig. 5 shows an example whose results are plotted in Fig. 6 (c). The DCE MRI data had simulated free-breathing motions which deformed the images. The four datasets had different magnitudes of motions. The images from different time points were all registered to a reference image, the MR image without enhancement, to correct the deformations in the liver. We calculated the warping index on the liver region.

Results: Fig. 6 plots the registration results. SIEMI performed evidently better than NMI, particularly between time points 5 to 10 when the contrast agent started to enter the liver region and changed the intensity values. The results also show that during the time points 1 to 5 when the contrast agent had not yet arrived the liver to change the intensity, NMI achieved similar warping indexes as SIEMI. From time point 10 to 15, the contrast agent in the liver was in late enhancement and the intensity distributions were more uniform. Therefore, NMI started to perform better than in the time points of enhancing. However, the accuracy was still not as good as that of SIEMI because there was still INU in the data due to the enhancement.

4 Conclusion

We have presented a new method, spatial information encoded mutual information measure (SIEMI), for nonrigid registration. This registration approach is based on the general spatial information encoding framework. We achieved the encoding using a weighting scheme to differentiate the contribution of pixels to the set of entropy measures which are associated with the spatial variable. The similarity measure of SIEMI is a vector which consists of the set of entropy measures. To efficiently search the optimum of this measure, we proposed to use the local ascent optimization scheme. The result showed that the local ascent was able to converge to similar accuracy and save up to two orders of magnitude computation time compared to the registration using the global ascent scheme.

SIEMI was particularly proposed to tackle the nonrigid registration problems caused by the intensity non-uniformity (INU) or enhancement in the images. We validated the method using brain MR data with different level of INU and dynamic contrast enhancement MRI of the liver. The results showed that SIEMI well overcame the problems and performed significantly better than the registration using normalized mutual information.

Acknowledgement

Xiahai Zhuang was funded by EPSRC grant GR/T11395/01. The authors thank Dr. Andrew Melbourne and Dr. David Atkinson for providing the DCE MRI.

References

1. Viola, P., Wells, III, V.M.: Alignment by maximization of mutual information. International Journal of Computer Vision **24**(2) (1997) 137–154
2. Maes, F., Collignon, A., Vandermeulen, D., Marchal, G., Suetens, P.: Multimodality image registration by maximization of mutual information. IEEE Transactions of Medical Imaging **16**(2) (April 1997) 187–198
3. Wells III, W.M., Viola, P., Atsumi, H., Nakajima, S., Kikinis, R.: Multi-modal volume registration by maximisation of mutual information. Medical Image Analysis **1**(1) (1996) 35–51

4. Studholme, C., Hill, D.L.G., Hawkes, D.J.: An overlap invariant entropy measure of 3D medical image alignment. Pattern Recognition **32**(1) (Jan 1999) 71–86
5. Rueckert, D., Sonoda, L.I., Hayes, C., Hill, D.L.G., Leach, M.O., Hawkes, D.J.: Nonrigid registration using free-form deformations: Application to breast MR images. IEEE Transactions on Medical Imaging **18** (1999) 712–721
6. Pluim, J.P.W., Maintz, J.B.A., Viergever, M.A.: Mutual information based registration of medical images: A survey. IEEE Transaction on Medical Imaging **22**(8) (2003) 986–1004
7. Studholme, C., Drapaca, C.S., Iordanova, B., Cardenas, V.: Deformation-based mapping of volume change from serial brain MRI in the presence of local tissue contrast change. IEEE Transactions on Medical Imaging **25**(5) (2006) 626–639
8. Loeckx, D., Slagmolen, P., Maes, F., Vandermeulen, D., Suetens, P.: Nonrigid image registration using conditional mutual information. In: Information Processing in Medical Imaging, Volume 4584 of LNCS (2007) 725–737
9. Loeckx, D., Slagmolen, P., Maes, F., Vandermeulen, D., Suetens, P.: Nonrigid Image Registration Using Conditional Mutual Information. IEEE Transactions on Medical Imaging **29**(1) (2010) 19–29
10. Zhuang, X., Hawkes, D.J., Ourselin, S.: Unifying encoding of spatial information in mutual information for nonrigid registration. In: Information Processing in Medical Imaging, Volume 5636 of LNCS (2009) 491–502
11. Melbourne, A., Atkinson, D., White, M.J., Collins, D., Leach, M., Hawkes, D.: Registration of dynamic contrast-enhanced MRI using a progressive principal component registration (ppcr). Physics in Medicine and Biology **52** (2007) 5147–5156
12. Li, C., Sun, Y.: Nonrigid registration of myocardial perfusion MRI using pseudo ground truth. In: MICCAI, Volume 5761 of LNCS (2009) 165–172
13. Hermosillo, G., Chefd'Hotel, C.C., Faugeras, O.D.: Variational methods for multimodal image matching. International Journal of Computer Vision **50**(3) (2002) 329–343
14. Pluim, J.P.W., Maintz, J.B.A., Viergever, M.A.: Interpolation artefacts in mutual information-based image registration. Computer Vision and Image Understanding **77**(2) (2000) 211–232
15. Likar, B., Pernus, F.: A hierarchical approach to elastic registration based on mutual information. Image and Vision Computing **19** (2001) 33–44
16. Zhuang, X., Rhode, K., Razavi, R., Hawkes, D.J., Ourselin, S.: A registration-based propagation framework for automatic whole heart segmentation of cardiac MRI. IEEE Transactions on Medical Imaging (In Press), vol.PP, no.99, pp.1-1, 0 doi: 10.1109/TMI.2010.2047112
17. Zhuang, X., Rhode, K., Arridge, S., Razavi, R., Hill, D., Hawkes, D., Ourselin, S.: An atlas-based segmentation propagation framework using locally affine registration – application to automatic whole heart segmentation. In MICCAI, Volume 5242 of LNCS (2008) 425–433
18. Schnabel, J.A., Rueckert, D., Quist, M., Blackall, J.M., Castellano-Smith, A.D., Hartkens, T., Penney, G.P., Hall, W.A., Liu, H., Truwit, C.L., Gerritsen, F.A., Hill, D.L.G., Hawkes, D.J.: A generic framework for non-rigid registration based on non-uniform multi-level free-form deformations. In: MICCAI, Volume 2208 of LNCS (2001) 573–581
19. Klein, S., Staring, M., Pluim, J.P.W.: Evaluation of optimization methods for nonrigid medical image registration using mutual information and B-splines. IEEE Trans. Image Processing **16**(12) (2007) 2879–2890
20. Rueckert, D., Aljabar, P., Heckemann, R.A., Hajnal, J.V., Hammers, A.: Diffeomorphic registration using b-splines. In: MICCAI, LNCS 4191, (2006) 702–709